Analytical Investigation of Frequency Behavior in Tunnel Injection Quantum Dot VCSEL

Mehd Riahinasab[1] , Elham Darabi[*, 2]

[1] Department of Electrical Engineering, Science and Research Branch, Islamic Azad University, Tehran, Iran

[2] Plasma physics research center, Science and Research Branch, Islamic Azad University, Tehran, Iran.

Abstract: The frequency behavior of the tunnel injection quantum dot vertical cavity surface emitting laser (TIQD-VCSEL) is investigated by using an analytical-numerical method on the modulation transfer function. The function is based on the rate equations and is decomposed into components related to different energy levels inside the quantum dot and injection well. In this way, the effect of the tunneling process on the improvement of the laser frequency response is determined. Generally, the components of the modulation transfer function in the wetting layer and the excited state limit the total laser bandwidth. Of course, the component associated with the tunneling process increases overall system bandwidth. It is shown that for currents above threshold, the carrier density at the excited state in TIQD has a slight slope, unlike the conventional quantum dot (CQD). It will improve the frequency response of the tunnel injection structure. It can be attributed to the difference in Pauli blocking factor values at the excited state and the ground state in the two structures.

Keywords: Modulation Transfer Function, Tunnel Injection Quantum Dot (TIQD), Vertical Cavity Surface Emitting Laser (VCSEL).

---

* Corresponding author. Email: **e.darabi@srbiau.ac.ir**

1. INTRODUCTION

In comparison with other lasers including bulk ones and quantum well, quantum dot semiconductor lasers have more remarkable advantages. High differential gain [1, 2], low threshold current [3, 4], no temperature sensitivity of threshold current [5, 6], and high power output [7] can be referred to as the main advantages of QD lasers. However, because of phonon bottleneck in the carriers capturing process leading to a hot carrier problem, such lasers cannot operate well in high frequencies [8, 9]. The impact of the hot carrier due to the gain compression can decrease differential gain [10]. Effect of the gain compression limits the resonance frequency and consequently the modulation bandwidth of laser. In other words, the finite rate of capture and relaxation of the carrier [11] is the main reason which limits the operation of the quantum dot lasers in high frequencies. Direct injection of the carrier to the ground state of quantum dots can be considered as a practical solution. First, it was used for semiconductor quantum well lasers. The studies showed that direct tunneling of cold electron from an injector well into the lasing band of quantum well lasers can improve the characteristics of the laser. These features include improvement of the modulation bandwidth, increase in characteristic temperature T0, and decrease of auger recombination [12-14]. In addition, the tunnel injection technique was used in quantum dot lasers, and a small signal modulation up to a frequency of 20GHz was achieved [15-17]. In a tunnel injection quantum dot structure, electrons are directly or through phonon-assisted entered into lasing states of quantum dots. It decreases the impact of the hot carrier and gain compression. In the tunnel injection structure, tunneling rate is an effective parameter on the resonance frequency and damping factor. Therefore, appropriate designing of the injector well, the thickness and height of the tunnel barrier can decrease tunneling time, and improve the operation of the laser in high frequencies.

This study proposes a modified analytical-numerical model by generalizing the method cited in [11], and simulates the frequency behavior of a vertical cavity surface emitting laser with a tunnel injection quantum dot structure. The impact of the dynamic carrier at different states of energy in the quantum dot and tunneling process on the bandwidth of the modulation transfer function is obtained. In TIQD structure, the component of modulation transfer function associated with tunneling process enjoys a high bandwidth. It neutralizes the limitation due to the modulation transfer function associated with the wetting layer and excited state. As a result, it increases the modulation bandwidth of laser. In the given model, the impact of the passing and entering of carrier into the wetting layer would be assessed as well. Clearly, the frequency response of a VCSEL will change according to the structure and size of the laser as well as

depth and radius of the oxide aperture. Also, the carrier distribution and the temperature at the center of the active region are the most important parameters which affect the frequency response of the VCSEL. So, investigation of thermal phenomenon requires the evaluation of the self-heating effect and its outcomes. Coupled rate-temperature equations were solved by the self-consistent algorithm which is defined in [18]. This article is presented as follows. Section 2 deals with the analytical model to describe and study the dynamic carrier, and effective parameters in resonance frequency as well as the damping factor. As a result, a new modulation transfer function is obtained by analyzing of small signal differential rate equations. In section 3, the given TIQD-VCSEL structure is introduced. In Section 4, the analytical and numerical results of the given model are shown. In this paper, for the first time, by considering of the effects of carrier concentration and temperature in the active region, the bandwidths of modulation transfer functions associated with different levels of energy in dot and injector well are obtained. Also, the origin of the frequency behavior improvement in the TIQD is studied. In this manner, the effect of tunnel injection on the resonance frequency of TIQD laser is presented. These theoretical investigations are of prime importance for the optimization of low cost sources for optical telecommunications as well as for a further improvement of QD laser performances.

2. DESCRIPTION OF AN ANALYTICAL – NUMERICAL MODEL

Figure 1 indicates the schematic of the carrier dynamics in the conduction band. It includes tunnel injection from an injector well into quantum dots and dynamic carrier in energy levels of wetting layer and quantum dots. The operation of tunnel injection process is as follows: first, outside carriers are injected into the SCH layer, and entered into the injector well. Some of the carriers with a probability coefficient p_t are directly tunneled or through phonon energy into the ground state of quantum dots or with a probability coefficient $1 - p_t$ are entered into the wetting layer. Other carriers take part in spontaneous emission process with time rate τ_{spon-w}. In the wetting layer, carriers are captured into the energy excited state within time τ_{c1}, or they are directly captured into the energy state ground within time τ_{c0}. Some of them take part in the spontaneous emission process with time rate $\tau_{spon-WL}$. Carriers on the excited state relax into the ground state during τ_{10}. While others spread thermally from the excited state into the wetting layer during τ_{e1}. This happens following the Fermi Dirac Distribution with no external forces [19].

The dynamic behavior of carriers on the ground state is similar to the excited state. While some of them are spontaneously recombined during τ_s. In the

proposed model, stimulated emission of just the ground state will be calculated in terms of the presence of the threshold. While in this model the auger recombination has not been considered for the excited and ground states, because in room temperature most carriers are in the injector well and wetting layer [15].
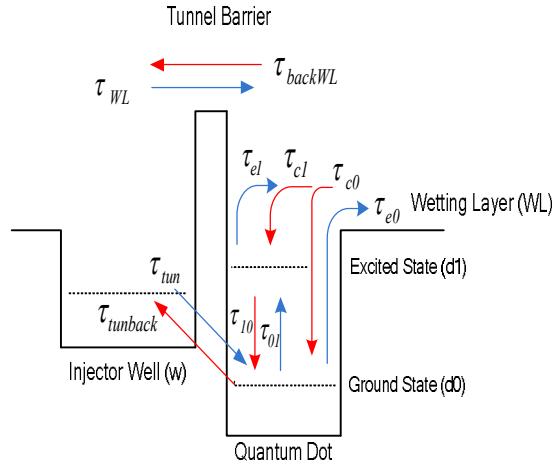
Fig. 1. Carrier Transport Process in the Tunnel Injection Quantum Dot Structure

For carriers tunneled into the ground state the probability is p_t, and for the ones directly entered into the wetting layer, the probability is $1 - p_t$. We assume that in this model a fraction of carriers within the injector well passes over the barrier and reaches to the wetting layer. From there, they transfer toward the QD ground state according to the carrier capture and relaxation process. Band gap of the injector well is set to provide the conditions for tunneling through barrier layer. In order to achieve high efficiency tunneling from the injector well into the quantum dots, conduction bands levels of the injector well need to be conformed to the quantum dots band levels [15]. In the proposed model assuming that the active region includes just a unit of homogeneous quantum dots which has two energy levels: a ground state with two degenerate states, and an excited state with four degenerate states. In this system, energy states are excitonic. Following the sketch in figure 1, the carrier dynamic defined with a set of rate equations given by [15] is modified by considering the effect of carrier passing into the WL as follows:

$$\frac{dN_w}{dt} = \frac{J}{qd} + p_t \cdot \frac{N_w}{\tau_{tun}} \cdot \left(1 - \frac{N_{d0}}{2N_d}\right) + p_t \cdot \frac{N_{d0}}{\tau_{tunback}} - \frac{N_w}{\tau_{spon-w}} - (1 - p_t) \cdot \frac{N_w}{\tau_{WL}} + (1 - p_t) \cdot \frac{N_b}{\tau_{backWL}}$$

$$\frac{dN_{WL}}{dt} = -\frac{N_{WL}}{\tau_{c1}} \cdot \left(1 - \frac{N_{d1}}{4N_d}\right) + \frac{N_{d1}}{\tau_{e1}} - \frac{N_{WL}}{\tau_{c0}} \cdot \left(1 - \frac{N_{do}}{2N_d}\right) + \frac{N_{d0}}{\tau_{e0}} - \frac{N_{WL}}{\tau_{spon-WL}} + (1-p_t) \cdot \frac{N_w}{\tau_{WL}} - (1-p_t) \cdot \frac{N_{WL}}{\tau_{backWL}}$$

$$\frac{dN_{d1}}{dt} = -\frac{N_{d1}}{\tau_{10}} \cdot \left(1 - \frac{N_{d0}}{2N_d}\right) + \frac{N_{d0}}{\tau_{01}} \cdot \left(1 - \frac{N_{d1}}{4N_d}\right) - \frac{N_{d1}}{\tau_{e1}} + \frac{N_{WL}}{\tau_{c1}} \cdot \left(1 - \frac{N_{d1}}{4N_d}\right)$$

$$\frac{dN_{d0}}{dt} = p_t \cdot \frac{N_W}{\tau_{tun}} \cdot \left(1 - \frac{N_{d0}}{2N_d}\right) - p_t \cdot \frac{N_{d0}}{\tau_{tunback}} + \frac{N_{d1}}{\tau_{10}} \cdot \left(1 - \frac{N_{d0}}{2N_d}\right) + \frac{N_{WL}}{\tau_{c0}} \cdot \left(1 - \frac{N_{d0}}{2N_d}\right) - \frac{N_{d0}}{\tau_{e0}} - \frac{N_{d0}}{\tau_{01}} \cdot \left(1 - \frac{N_{d1}}{4N_d}\right) - \frac{N_{d0}}{\tau_s} - g \cdot v_g \cdot S$$

$$\frac{dS}{dt} = \Gamma_p \cdot g \cdot v_g \cdot S - \frac{S}{\tau_p} + \Gamma_p \cdot \beta_{sp} \cdot \frac{N_{d0}}{\tau_s} \tag{1}$$

N_w, N_{WL}, N_{d1} and N_{d0} are respectively the carrier concentration in the injector well, wetting layer, excited state, and ground state of the quantum dots. S is the density of photon inside the cavity laser. β_{sp} and Γ_p are spontaneous emission coefficient and optical confinement factor respectively. τ_p equals photon lifetime, v_g is the group velocity, and d is the thickness of the active region. The probability of having a state with no carrier in the GS and ES known as Pauli blocking factors is defined as follows [11]:

$$f_{gs} = 1 - \frac{N_{d0}}{2N_d} \quad , \quad f_{es} = 1 - \frac{N_{d1}}{4N_d} \tag{2}$$

Optical gain inside cavity can be defined as a function of the carrier concentrations in the ground state and generated photon.

$$g = g_0 \cdot N_d \cdot \left(\frac{N_{d0}}{N_d} - 1\right) \cdot \frac{1}{1 + \varepsilon S} \tag{3}$$

g_0 coefficient is considered as differential gain. N_d is the total number of quantum dots. ε is the gain compression factor which indicates changes of optical gain associated with photon density.

The gain changes as a dynamic variable dependent to the carrier and photon density are given by $dg = g_0 dN_{d0} - g_s dS$ in which $g_s = -\frac{\partial g}{\partial S}$ and $g_0 = \frac{\partial g}{\partial N_{d0}}$. In order to show the dependency of gain to the photon density, the gain compression factor can be used instead of g_s [10]. Then in (3), the relationship ε and g_s is given by $g_s = \frac{\varepsilon g}{1 + \varepsilon S}$.

It is worth mentioning that the differential gain (g_0) and gain compression factor (ε) are given physical quantities that their values can be calculated by the characteristics of the laser. While, optical gain (g) and gain derivation by the number of photons are not unique parameters, because their values are calculated based on the radial dependence of the carriers concentration. Applying a small signal dynamic model of variables N_{d0}, N_{d1}, N_{WL}, N_W, and I as well as gain (g), and derivation of the above differential equations, the matrix

equation model for the small signal response to sinusoidal current at the modulation frequency $\omega/2\pi$ is obtained as follows:

$$
\begin{bmatrix}
j\omega+\gamma_{11} & -\gamma_{12} & 0 & -\gamma_{14} & 0 \\
-\gamma_{21} & j\omega+\gamma_{22} & -\gamma_{23} & -\gamma_{24} & 0 \\
0 & -\gamma_{32} & j\omega+\gamma_{33} & -\gamma_{34} & 0 \\
-\gamma_{41} & -\gamma_{42} & -\gamma_{43} & j\omega+\gamma_{44} & -\gamma_{45} \\
0 & 0 & 0 & -\gamma_{54} & j\omega+\gamma_{55}
\end{bmatrix}
\cdot
\begin{bmatrix}
N_w \\ N_b \\ N_{d1} \\ N_{d0} \\ S
\end{bmatrix}
= \frac{I}{qd} \cdot
\begin{bmatrix}
1 \\ 0 \\ 0 \\ 0 \\ 0
\end{bmatrix}
\tag{4}
$$

with

$$
\gamma_{11} = \frac{f_{gs} \cdot p_t}{\tau_{tun}} + \frac{1}{\tau_{spon\_w}} + \frac{1-p_t}{\tau_{WL}} \quad ; \quad \gamma_{12} = \frac{1-p_t}{\tau_{WL}} \quad ; \quad \gamma_{14} = \frac{p_t}{\tau_{tunback}} \quad ; \quad \gamma_{21} = \frac{1-p_t}{\tau_{WL}}
$$

$$
\gamma_{22} = \frac{f_{es}}{\tau_{c1}} + \frac{f_{gs}}{\tau_{c0}} + \frac{1}{\tau_{spon\_WL}} + \frac{1-p_t}{\tau_{backWL}} \quad ; \quad \gamma_{23} = \frac{1}{\tau_{e1}} \quad ; \quad \gamma_{24} = \frac{1}{\tau_{e0}} \quad ; \quad \gamma_{32} = \frac{f_{es}}{\tau_{c1}}
$$

$$
\gamma_{33} = \frac{f_{gs}}{\tau_{10}} + \frac{1}{\tau_{e1}} \quad ; \quad \gamma_{34} = \frac{f_{es}}{\tau_{01}} \quad ; \quad \gamma_{41} = \frac{p_t \cdot f_{gs}}{\tau_{tun}} \quad ; \quad \gamma_{42} = \frac{f_{gs}}{\tau_{c0}} \quad ; \quad \gamma_{43} = \frac{f_{gs}}{\tau_{10}}
$$

$$
\gamma_{44} = \frac{p_t}{\tau_{tunback}} + \frac{1}{\tau_{e0}} + \frac{f_{es}}{\tau_{01}} + \frac{1}{\tau_s} + v_g \cdot g_0 \cdot S \quad ;
$$

$$
\gamma_{45} = v_g \cdot g_s \cdot S - v_g \cdot g \quad ; \quad \gamma_{54} = \frac{\Gamma_p \cdot \beta_{sp}}{\tau_s} + \Gamma_p \cdot v_g \cdot g_0 \cdot S
$$

$$
\gamma_{55} = \Gamma_p \cdot v_g \cdot g_s \cdot S - \Gamma_p \cdot v_g \cdot g + \frac{1}{\tau_p}
\tag{5}
$$

The modulation transfer function is defined as [11]:

$$
H_{TIQD} = \frac{R_0}{\Delta} = \frac{R_0}{j\omega^5 + R_4\omega^4 - R_3 j\omega^3 - R_2\omega^2 + R_1 j\omega + R_0}
\tag{6}
$$

In this relation, Δ is the determinant of the coefficient matrix, R parameters obtained based on the coefficient matrix. The relaxation resonance frequency and damping factor of the lasing level are obtained by the matrix coefficients as:

$$
\omega_R^2 = \gamma_{44}\gamma_{55} - \gamma_{45}\gamma_{54}
\tag{7}
$$

$$\Gamma = \gamma_{44} + \gamma_{55}$$

Similarly, the relaxation resonance frequency and damping factor related to the carrier capture and relaxation are defined as:

$$\omega_{R_0}^2 = \gamma_{22}\gamma_{33} - \gamma_{23}\gamma_{32} \ , \qquad \Gamma_0 = \gamma_{22} + \gamma_{33} \tag{8}$$

Deleting the small components of R parameters, we can simplify their definitions as follows:

$$R_0 = \gamma_{11}\omega_R^2\omega_{R_0}^2 - \gamma_{12}\gamma_{21}\gamma_{33}\omega_R^2$$

$$R_1 = \gamma_{12}\gamma_{21}\gamma_{33}\omega_R^2 - \gamma_{12}\gamma_{21}\gamma_{33}\Gamma + \gamma_{11}\Gamma\omega_{R_0}^2 + \gamma_{11}\Gamma_0\omega_R^2 + \omega_R^2\omega_{R_0}^2$$

$$R_2 = \gamma_{11}\omega_{R_0}^2 + \gamma_{11}\Gamma\Gamma_0 + \omega_{R_0}^2\Gamma + \omega_R^2\cdot(\gamma_{11}+\Gamma) - \gamma_{12}\gamma_{21}\cdot(\gamma_{33}+\Gamma)$$

$$R_3 = \gamma_{11}\cdot(\Gamma+\Gamma_0) + \Gamma\Gamma_0 + \omega_R^2 + \omega_{R_0}^2 - \gamma_{12}\gamma_{21}$$

$$R_4 = \gamma_{11} + \Gamma + \Gamma_0 \tag{9}$$

Based on this simplification, the modulation transfer function of the relation (6) is approximated as follows:

$$H_{app}(\omega) = H_{stim}(\omega)\cdot H(\omega) \tag{10}$$

Where

$$H_{stim}(\omega) = \frac{\omega_R^2}{(\omega_R^2 - \omega^2 + j\omega\Gamma)} \tag{11}$$

$$H(\omega) = \frac{\gamma_{11}\omega_{R_0}^2 - \gamma_{12}\gamma_{21}\gamma_{33}}{(j\omega+\gamma_{11})\cdot(\omega_{R_0}^2 - \omega^2 + j\omega\Gamma_0) - \gamma_{12}\gamma_{21}(j\omega+\gamma_{33})} \tag{12}$$

In the above relation, $H_{stim}(\omega)$ represents the modulation transfer function of the lasing level and $H(\omega)$ represents the whole area of tunneling and carrier relaxation. Clearly, effective parameters on the modulation transfer function $H(\omega)$ including time constants in the wetting layer (WL), excited state (ES), ground state (GS), tunneling time into GS and Pauli blocking factors at the GS and ES (f_{es}, f_{gs}). Regardless of the components γ_{12} and γ_{12}, the $H(\omega)$ function can be divided into two parts: $H_{WL-ES}(\omega)$ and $H_{tun}(\omega)$. Each represents the modulation transfer function at WL, ES and tunneling process. Then the function $H_{app}(\omega)$ is rewritten as follows:

$$H_{app}(\omega) = H_{stim}(\omega)\cdot H_{WL-ES}(\omega)\cdot H_{tun}(\omega) \tag{13}$$

where

$$H_{stim}(\omega) = \frac{\omega_R^2}{(\omega_R^2 - \omega^2 + j\omega\Gamma)} \tag{14}$$

$$H_{WL-ES}(\omega) = \frac{\omega_{R_0}^2}{(\omega_{R_0}^2 - \omega^2 + j\omega\Gamma_0)} \tag{15}$$

$$H_{tun}(\omega) = \frac{\gamma_{11}}{(j\omega + \gamma_{11})} \tag{16}$$

In the definition of $H_{WL-ES}(\omega)$ and $H_{tun}(\omega)$, the impact of the carriers passing from the injector well into the wetting layer for $p_t \neq 1$ can be seen in the components γ_{11} and γ_{22}. Regardless of the components γ_{12} and γ_{21}, it doesn't show a great impact on the 3dB frequency of the function $H(\omega)$ comparing with the multiplication of the two functions of $H_{WL-ES}(\omega)$ and $H_{tun}(\omega)$.

Then for all values of p_t $(0 < p_t < 1)$, the behavior of $H_{WL-ES}(\omega)$ and $H_{tun}(\omega)$ can be discussed. So if $p_t = 1$ (regardless of the passing of the carrier into the wetting layer), the function $H(\omega)$ can exactly be divided into two parts: $H_{WL-ES}(\omega)$ and $H_{tun}(\omega)$. Considering the obtained relations for the resonance frequency and damping factor at the lasing and relaxation levels, not only time constants are seen to have an impact on the frequency behavior of the laser but also some parameters like gain (g), photon density (S), carrier concentration at the excited state (N_{d1}), and the ground state (N_{d0}) as well as their Pauli blocking factors (f_{gs}, f_{es}). These parameters are dependent on the structure of the active region of the VCSEL. In order to exactly calculate these parameters, coupled equations of the carrier concentration and thermal alongside the whole radial points of the active region of the VCSEL are considered.

3. STRUCTURE

The basic structure which has been used is a VCSEL with wavelength *1.3μm* (See figure 2) and has the following parts [18]:
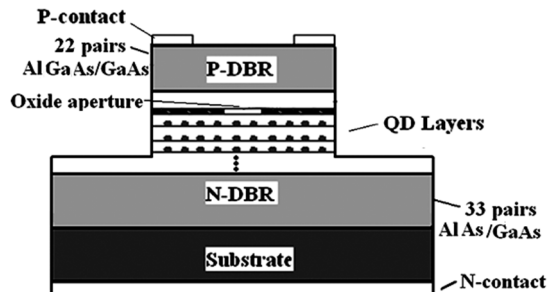
Fig. 2. Schematic diagram of TIQD-VCSEL model

The top and bottom DBR mirrors have impurity concentrations of 5×10^{17}cm^{-3} and 1×10^{18}cm^{-3} with 22 and 33 periods comprising layers with a quarter wavelength of GaAs/Al$_{0.8}$Ga$_{02}$As, and GaAs/AlAs. A layer of Al$_x$O$_y$ with 20nm thickness has been located next to the active region as a selectively oxidized with a determined oxide aperture diameter. Metal contacts have been set on the bottom and top DBRs. The active region has been considered based on the model similar to the tunnel injection quantum dot active region structure in Ref. [15].

The scheme of this structure is shown in figure 3 and the energy schematic of this model is shown in figure 4. In order to evaluate the mechanism of the tunneling injection quantum dot as well as its advantages, we compare it with the conventional quantum dot (CQD) (the structure of the quantum dot inside the well [18]), and the related equations.
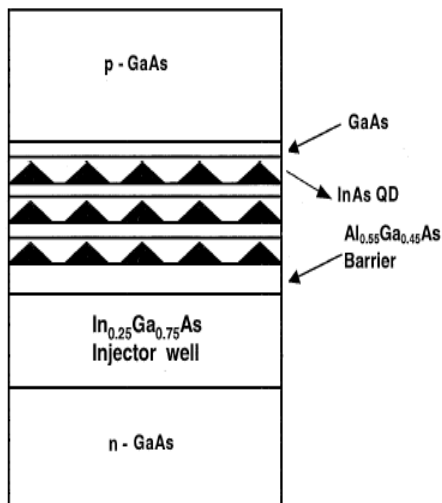
Fig. 3. Arrangement of the injector well, and the layers of the quantum dots within the active region [15]
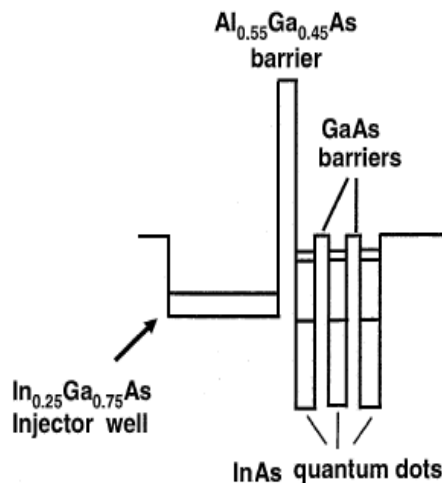
Fig. 4. The Energy Schematic of the given Model of the Mechanism of Tunneling Injection from an Injector Well into the Ground State of Quantum Dots [15]

The active region consists of an $In_{0.25}Ga_{0.75}As$ injector well with a thickness of 9.5nm, a $Al_{0.55}Ga_{0.45}As$ tunnel barrier with a 2nm thickness, several layers of self-assembled coupled InAs-GaAs quantum dots with a surface concentration of $\rho=5\times10^{10}cm^{-2}$. The number of optimal quantum dots, the thickness of each layer, the surface concentration of the quantum dots in each layer and the sizes

of the quantum dots are designed according to the output characteristics including the light emission wavelength, conditions to access the minimum threshold current and temperature. In order to emit light with a wavelength of about 1300nm, the sizes of pyramid-shaped quantum dots are obtained based on the theoretical calculations of the band structure for both the valence and conduction states using the *8band-k.p* model [20]. The calculations show that the width of each pyramid equals 11.8nm, the height 5.6nm, and the thickness of wetting layer is 1nm. The energy gap of the injector well and the quantum dots are 1.42ev and 0.35ev, respectively. The energy levels computed at the conduction and valence bands of the InAs-GaAs quantum dot is presented in figure 5. According to the figure, there are a number of close energy states for holes. Electrons have discrete states, so the difference between energy states of the first excited and ground state is about 100 meV. This energy difference is larger than the light phonon energy. In conclusion, the phonon scattering mechanism, which is the main cause of the rapid carrier relaxation in the injector well structure, is limited to the quantum dots. Then carrier relaxation time highly increases in the quantum dots. This article is to analytically evaluate this limitation and its improvement via a tunneling injection mechanism. The carrier relaxation rate in the quantum dot is calculated as the following relation:

$$\tau_{i,j} = \frac{1}{A_{i,j} + C_{i,j} N_{WL}} \tag{17}$$
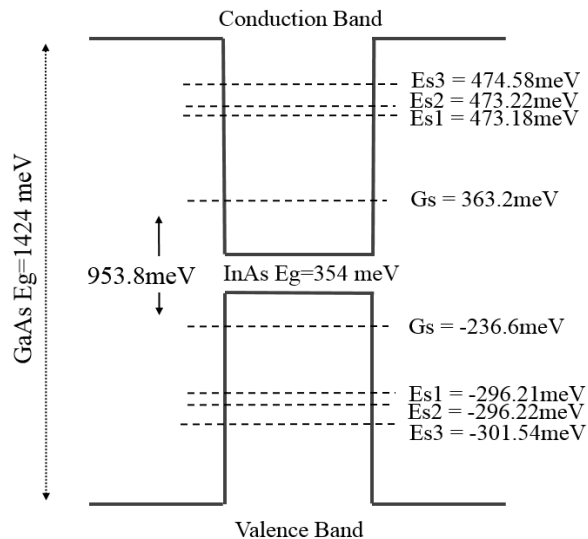
Fig. 5. Energy levels of valence and conduction bands of an InAs-GaAs Quantum Dot

$A_{i,j}$ and $C_{i,j}$, respectively represent the phonon-assisted carrier relaxation rate and Auger relaxation coefficient between i state and j levels. Subscripts of i and j are 0 and 1 and WL represents the ground state, first excited state, and the lowest energy states of the wetting layer. N_{WL} is the carrier concentration of the wetting layer.

The values of $A_{i,j}$ and $C_{i,j}$ are based on the reference [21] and are listed in Table 1. The escape rate of the carrier from the ground state to the excited state and from the excited stated to the wetting layer is according to the carrier transfer in the relaxation and capture processes. The proportionality coefficients of η_{GS-ES} and η_{ES-WL} are shown as follows [22]:

$$\eta_{GS-ES} = \frac{\rho_{GS}}{\rho_{ES}} \exp(\frac{\Delta E_{ES-GS}}{K_B T}) \tag{18}$$

$$\eta_{ES-WL} = \exp(\frac{\Delta E_{WE-ES}}{K_B T}) \tag{19}$$

In these relations, ΔE_{ES-GS} and ΔE_{WE-ES} respectively show the energy difference between the ground state and the excited state as well as between the excited state and the wetting layer. Also, $\rho_{GS} = 2$ and $\rho_{ES} = 4$ are for degenerate states in ground state and the excited state, respectively.

By neglecting the temperature variation in the longitudinal direction, the thermal conduction equation in steady state is given by [18]:

$$\frac{1}{r}\frac{\partial}{\partial r}(r\frac{\partial T}{\partial r}) + \frac{1}{\lambda_i}Q(J,r) = 0 \tag{20}$$

λ_i represents the thermal conductivity coefficient. $Q(J,r)$ equals the density of the total generated heating in the laser including Joule heating in DBR layers, absorption of spontaneous emission, and non-radiative recombination in the active region. The definitions of the components including the density of the generated heat in the laser, the spread of the current and voltage in the active region, and the parameters used in this model are based on the approach of the [18]. Definitions of the parameters of model and the values of time constants of the figure 1 are shown in the Table1.

TABLE1
Time Constants and the Parameters used in the Model

Parameter	Symbol	Value	Unit	Ref.
Capture Time from WL to ES	τ_{c1}	7	ps	--
Capture Time from WL to GS	τ_{c0}	15	ps	--
Relaxation Time from ES to GS	τ_{10}	--	ps	--
Tunneling Time to GS	τ_{tun}	0.5-2	ps	--
Capture Time to WL	τ_{WL}	1.7	ps	--
Spontaneous emission factor	β_{sp}	1×10^{-8}	--	[15]
Optical confinement factor	Γ_p	0.06	--	[11]
Radiative recombination time	τ_s	2	ns	[15]
group velocity	v_g	8.5×10^7	m/s	[18]
photon lifetime	τ_p	12	ps	[11]
Spontaneous Emission Time of WL	$\tau_{spon-WL}$	400	ps	[11]
Spontaneous Emission Time of well	τ_{spon-w}	400	ps	[11]
Phonon assisted coefficient in ES	A_c	0.4×10^{12}	s^{-1}	[21]
Auger coefficient in ES	C_c	4×10^{-14}	m^3s^{-1}	[21]
Phonon assisted coefficient in GS	A_0	4×10^{11}	s^{-1}	[21]
Auger coefficient in GS	C_0	7.6×10^{-14}	m^3s^{-1}	[21]

4. RESULTS

First, the operation of the VCSEL in the steady state has been assessed by the numerical solution of the carrier diffusion and temperature equations. The conditions for the minimum threshold of the laser operation and carrier concentration changes during the currents above threshold have been determined. Then, the frequency behavior of VCSEL, are assessed according to the above mentioned analytical calculations. The carrier diffusion equations are obtained by adding the components of ∇^2N_w and ∇^2N_{WL}. The non-linear Newton method is used to determine the radial profile of the carrier. Thermal equation is solved by the Finite Difference Method, while considering Dirichlet boundary conditions.

One of the effective parameters on the threshold current is the number of the quantum dots layers. In the proposed model, the minimum threshold current is 4.9mA with 9 layers for CQD and 4.1mA with 3 layers for TIQD. It should be mentioned that in the tunnel injection structure, the number of the optimal quantum dots layers is less than the injector well quantum dots. If the number of quantum dots layers excessively increases, there will be no appropriate tunneling process from the injector well into the quantum dots layers. It leads to the increase of the threshold current. Also, in the reference [15], the number of quantum dots layers for the effective tunneling process is considered to be 3. Figure 6(a,b) depicts the carrier concentration at the excited and ground states. The insets show the photon density versus the injected current for CQD, and TIQD structure.

(a)   (b)
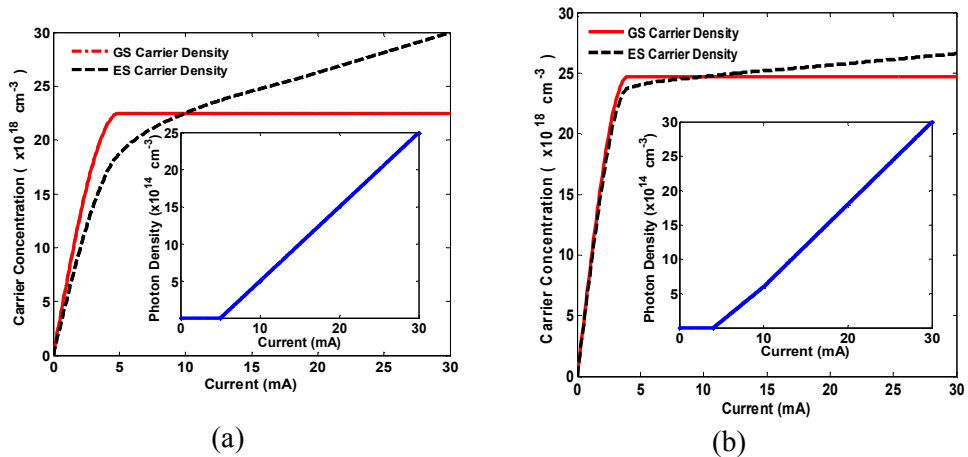
Fig. 6. The carrier concentration at the excited and ground states versus injected current in the two structures: (a) CQD and (b) TIQD. The insets show the photon density versus current.

As shown, by increment of current, the carrier concentration increases at the excited and ground states. So, in currents larger than 4.9mA and 4.1mA (the thresholds of the two structures), the carrier concentration at the ground state remains constant which leads to the lasing stimulated emission at the ground state. The difference between these two structures is in their carrier concentration at the excited state. In the CQD structure, the carrier concentration at the excited state is increasing with no slight slope. However, the carrier concentration in the tunnel injection structure has a slight slope at this case. The reason is that a great number of carriers are in the tunneling

process to reach to the lasing state. So, the excited state is not so effective in changing the carrier concentration. The result of this will affect the frequency response which will be explained later.

The components of the approximate solutions of the function $H_{app}(\omega)$ in the relations of (14) to (16) are depicted in figure 7 for the following values of $p_t = 1$ and $p_t = 0.9$. In the inset, the exact modulation function of $H_{TIQD}(\omega)$ presented in the relation (6) and its approximate solution $H_{app}(\omega)$ (relation (13)) is shown as well. It clearly indicates that they are close to each other with an appropriate approximation. In the analyzed model, the bandwidth of the exact and approximate transfer functions equals 11.6GHz.
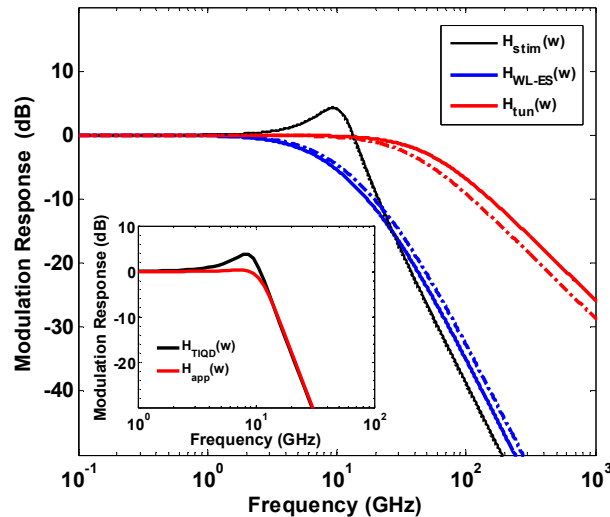
Fig. 7. The components of approximate solution of $H_{app}(\omega)$ for $p_t = 1$ (continuous line), and for $p_t = 0.9$ (discrete line) Internal shape: Exact modulation transfer function $H_{TIQD}(\omega)$, and Approximate solution $H_{app}(\omega)$.

Clearly, the frequency behavior of $H_{stim}(\omega)$ is similar to that of the transfer function in the quantum well structure and its 3db bandwidth is 15.3GHz. Between the components of the function $H_{app}(\omega)$, the $H_{WL-ES}(\omega)$ one with a 3dB bandwidth of 6.6GHz creates a limitation for the total modulation bandwidth. Of course, in the TIQD structure the dynamic carrier in the internal bands of the quantum dots do not have any significant effect on the function $H_{WL-ES}(\omega)$. While, in the CQD structure, the limited carrier capture and relaxation time physically limits the improvement of modulation bandwidth $H_{WL-ES}(\omega)$ [11]. This approves that the TIQD structure is preferable to the CQD structure. Additionally, the component $H_{tun}(\omega)$ has the highest 3dB bandwidth. It equals

52GHz (for tunneling time equals 1.7ns) which leads to the increase of the bandwidth of the whole system. Because this component is dependent on the tunneling time, for short tunneling time the laser modulation will be improved. If the probability coefficient of the carrier tunneling into the ground state (p_t) deceases, the 3dB bandwidth of the function $H_{tun}(\omega)$ decreases 37GHz and the 3dB bandwidth of $H_{WL-ES}(\omega)$ enhances to 7.5GHz. Although the bandwidth of the function $H_{stim}(\omega)$ does not show any significant change (about 200MHz).

In order to reveal the origin of such changes, we consider the dependency of the components comprising the transfer function to the time constants for CQD and TIQD structures. The modulation bandwidth of a function is highly dependent to its resonance frequency and damping factor. So, in order to evaluate the difference between CQD and TIQD, the resonance frequency and damping factor of $H_{stim}(\omega)$ and $H_{WL-ES}(\omega)$ are indicated as a function of the carrier relaxation time (τ_{10}) for different values of p_t (figures 8,9).

(a)   (b)
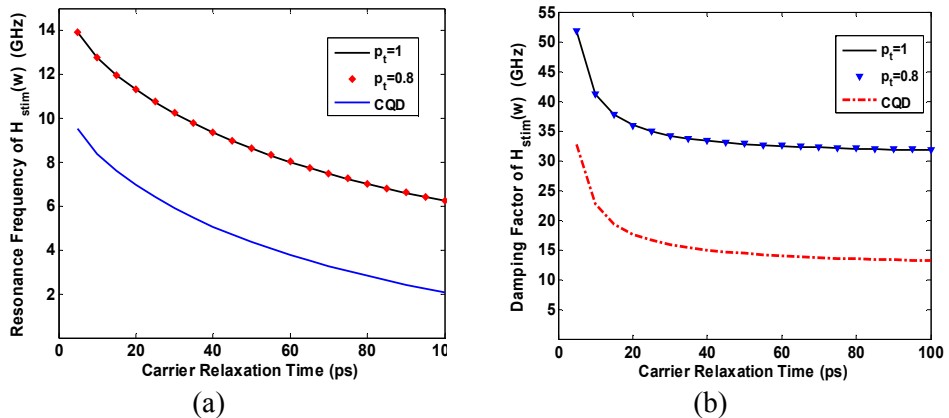
Fig. 8. (a) Resonance Frequency (b) Damping Factor of $H_{stim}(\omega)$ versus the Carrier Relaxation Time from ES to GS in the CQD-VCSEL and for Different Values of probability Coefficient in the TIQD-VCSEL

As indicated in the figure 8(a), if the relaxation time increases (5ps to 100ps), the resonance frequency of $H_{stim}(\omega)$ in both structures (TIQD and CQD) shows a uniform reduction of roughly 8GHz. By reducing the probability of carriers tunneling from the injector well into the GS of the quantum dots (p_t), the rate of reduction in the resonance frequency of $H_{stim}(\omega)$ is similar.
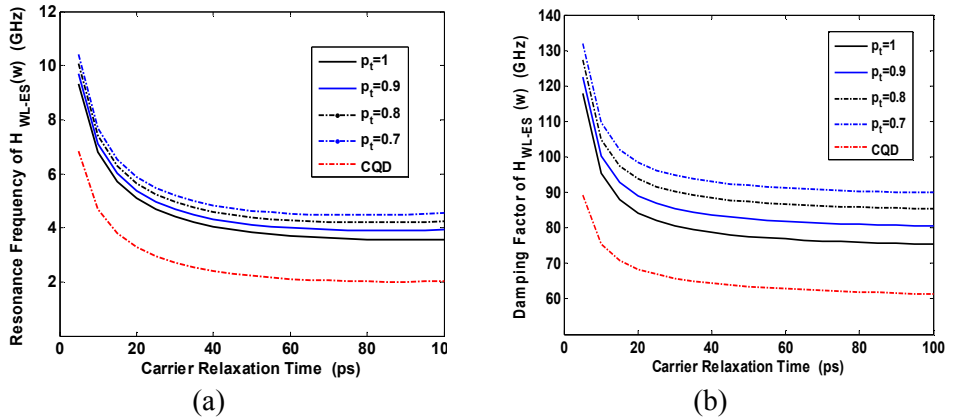
Fig. 9. (a) Resonance Frequency (b) Damping Factor of $H_{WL-ES}(\omega)$ versus the Carrier Relaxation Time from ES to GS in the CQD-VCSEL and for Different Values of probability Coefficient in the TIQD-VCSEL

Also, the figure 8(b) indicates that the decrease of the damping factor of $H_{stim}(\omega)$ based on τ_{10} in both structures shows a similar and independent of p_t. As the value of τ_{10} increases to 20ps, there is a sharp decrease of about 20GHz and then some slight changes. Similar evaluation of figure 9 indicates that the values of the resonance frequency and damping factor of $H_{WL-ES}(\omega)$ decrease as the carrier relaxation time increases. In addition, these parameters (f_{R0} and Γ_0) reversely correspond to the probability coefficient (p_t). The decrease of p_t can slightly enhance the f_{R0} and Γ_0.

Additionally, figure 9(b) shows that the reduction of damping Γ_0 versus the changes of τ_{10} in the TIQD structure is about 42GHz which is more than that of CQD (about 26GHz). While the reduction of the resonance frequency f_{R0} versus the changes of relaxation time is insignificant in both structures (for both of them, it decreases about 5GHz). It leads to the improvement of the $H_{WL-ES}(\omega)$ bandwidth. The impact of the relaxation process on the f_{R0} and Γ_0 can be attributed to the difference of Pauli blocking factor at the ES and GS (f_{es}, f_{gs}) which is described as follows.

The f_{gs} in TIQD is larger than that of CQD. On the other hand, with the changes of τ_{10}, the value of f_{es} in TIQD will remain constant. While, figure 10 indicates that in the CQD structure as τ_{10} increases, the f_{es} decreases. In this figure the changes of f_{es} versus the τ_{10} for different values of probability coefficient (p_t) are shown. According to expression of f_{es} and f_{gs} in Γ_0, it can be stated that the reduction of Γ_0 in TIQD is more than CQD. While, the changes of the resonance

frequency f_{R0} as a function of changes of the carrier relaxation time in both structures are similar, as the effect of f_{es} and f_{gs} on f_{R0} is not significant.

Therefore, in the TIQD, the amount of relaxation time in the internal band of QDs has less impact on the modulation bandwidth of $H_{WL-ES}(\omega)$. Obviously, with a given resonance frequency, the low damping factor can increase the 3dB bandwidth of the modulation transfer function.

The effect of the tunneling process on the bandwidth of $H_{stim}(\omega)$ can be attributed to the value of the Pauli blocking factor at the ES and GS (f_{es}, f_{gs}) as well as the generated photon density. As $\tau_{tunback}$ increases, there is roughly no tunnel back to the injector well. Then the carrier concentrations at the ES and GS as well as the possibility of finding a state with no carrier (which are the f_{es}, f_{gs}) indicate slight changes. So, they have less dependency to the values of τ_{tun}. To do more evaluation, the dependency of Pauli blocking factor at the GS (f_{gs}) to the τ_{tun} considering different values of $\tau_{tunback}$ are presented in figure 11. For the shorter tunnel back time, the longer the τ_{tun}, the greater the value of Pauli blocking factor at the ground state (f_{gs}). While, if the values of $\tau_{tunback}$ increase, the changes of f_{gs} versus the changes of τ_{tun} in the TIQD structure will remain constant.
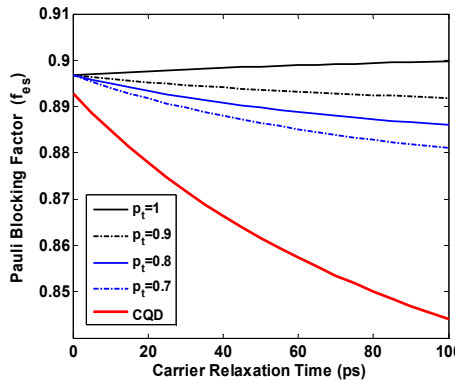
Fig. 10. The changes of Pauli blocking factor at the ES versus the carrier relaxation time for different values of probability coefficient in TIQD and CQD structures	**Fig. 11.** The changes of Pauli blocking factor at the GS as a function of the carrier relaxation time for 3 different values of tunnel back time
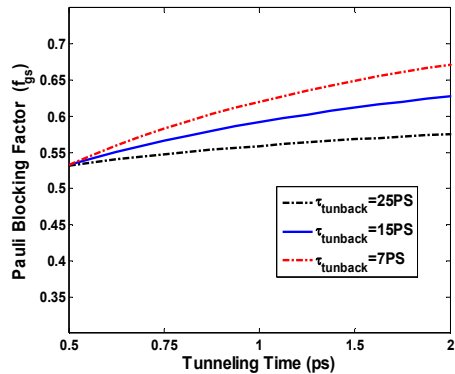
In conclusion, there are slight changes in the photon density of the cavity which are independent of the τ_{tun}. Also, with shorter tunneling time, the carrier concentration at the GS will be constant, due to the fast tunneling from the injector well. So, the photon density remains constant and independent of the $\tau_{tunback}$. Figure 12 shows the changes of the generated photon density as a

function of $\tau_{tunback}$ for two different values of τ_{tun}. As depicted, if $\tau_{tunback}$ increases, more photons are generated. Although for a small value of τ_{tun} , the dependency of the generated photon to the tunnel back time becomes weaker. In addition, the study shows that as $\tau_{tunback}$ increases, the dependency of the generated photon to τ_{tun} reduces. Therefore, considering two components of ω_R^2 and Γ in $H_{stim}(\omega)$ and their dependency to the photon density, $H_{stim}(\omega)$ has less dependency to τ_{tun} for greater values of $\tau_{tunback}$. Also as τ_{tun} decreases, the $H_{stim}(\omega)$ 3dB bandwidth is independent of $\tau_{tunback}$.
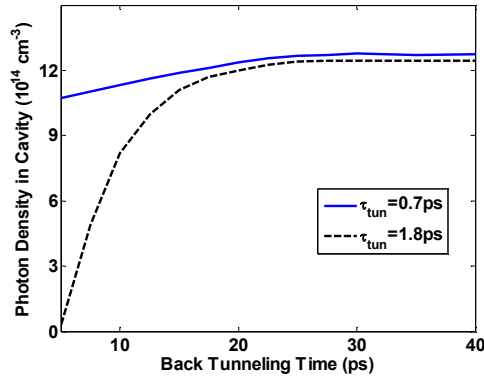
Fig. 12. The changes in the generated photon density as a function of the tunnel back time for two different values of tunneling time

5. CONCLUSION

Through the analysis of modulation transfer function, the characteristics of the tunneling injection quantum dot VCSEL were studied. By dividing of the function to detailed components, the origin of improving the frequency behavior of the laser was determined. In this model the bandwidth of modulation transfer functions related to energy levels in the quantum dot and injector well were obtained. In addition, the impact of the tunnel injection on the improvement of the frequency response was determined. The findings proved that the tunneling process would compensate the limitation of carrier dynamic in the wetting layer and the excited state. The damping factor of component related with the excited states and wetting layer levels had more changes in the tunnel injection structure. It led to the improvement of the bandwidth of the modulation transfer function of laser.

REFERENCES

[1] N. Kirstaedter, O. G. Schmidt, N. N. Ledentsov, D. Bimberg, V. M. Ustinov, A. Egorov, A. E. Zhukov, M. V Maximov, P. S. Kopev, and Z. Alferov. *Gain and differential gain of single layer InAs/GaAs quantum dot injection lasers*. Appl. Phys. Lett. 69(9) (1996) 1226–1228.
Available: https://aip.scitation.org/doi/10.1063/1.117419

[2] D. Klotzkin, K. Kamath, K. Vineberg, P. Bhattacharya, R. Murty, and J. Laskar. *Enhanced modulation bandwidth (20 GHz) of In/sub 0.4/Ga/sub 0.6/As-GaAs self-organized quantum-dot lasers at cryogenic temperatures: role of carrier relaxation and differential gain*. IEEE Photonics Technol. Lett. 10(7) (1998, July) 932–934. Available: https://ieeexplore.ieee.org/document/681274

[3] G. T. Liu, A. Stintz, H. Li, K. J. Malloy, and L. F. Lester. *Extremely low room-temperature threshold current density diode lasers using InAs dots in In0.15Ga0.85As quantum well*. Electron. Lett. 35 (1999) 1163–1165.
Available: https://pdfs.semanticscholar.org/29f5

[4] R. P. Sarzala. *Modeling of the threshold operation of 1.3-/spl mu/m GaAs-based oxide-confined (InGa)As-GaAs quantum-dot vertical-cavity surface-emitting lasers*. IEEE J. Quantum Electron. 40(6) (2004) 629–639.
Available: https://ieeexplore.ieee.org/document/1303776

[5] M. V Maksimov, N. Y. Gordeev, S. V Zaitsev, P. S. Kop'ev, I. V Kochnev, N. N. Ledentsov, A. V Lunev, S. S. Ruvimov, A. V Sakharov, A. F. Tsatsul'nikov, Y. M. Shernyakov, Z. I. Alferov, and D. Bimberg. *Quantum dot injection heterolaser with ultrahigh thermal stability of the threshold current up to 50 °C*. Semiconductors. 31(2) (1997, Feb.) 124–126.
Available: https://cip.cornell.edu/handle/cul.maik.sc/1214589781

[6] O. B. Shchekin and D. G. Deppe. *1.3m InAs quantum-dot laser with K from 0 to 80C*. Appl. Phys. Lett. 80 (2002) 3277–3279.

[7] D. Bimberg, M. Grundmann, F. Heinrichsdorff, N. N. Ledentsov, V. M. Ustinov, A. E. Zhukov, A. R. Kovsh, M. V Maximov, Y. M. Shernyakov, and B. V Volovik. *Quantum dot lasers: Breakthrough in optoelectronics*. Thin Solid Films. 367 (2000) 235–249. Available: https://www.sciencedirect.com/science/article/pii/

[8] M. H. Yavari and V. Ahmadi. *Effects of Carrier Relaxation and Homogeneous Broadening on Dynamic and Modulation Behavior of Self-Assembled Quantum-Dot Laser*. IEEE J. Sel. Top. Quantum Electron. 17(5) (2011, Sep.) 1153–1157.
Available: https://ieeexplore.ieee.org/document/5735155/

[9] J. Urayama, T. B. Norris, J. Singh, and P. Bhattacharya. *Observation of phonon bottleneck in quantum dot electronic relaxation*. Phys. Rev. Lett. 86(21) (2001, May) 4930–4933. Available: https://www.ncbi.nlm.nih.gov/pubmed/11384384

[10] A. Fiore and A. Markus. *Differential Gain and Gain Compression in Quantum-Dot Lasers*. IEEE J. Quantum Electron. 43(4) (2007, Mar.) 287–294.
Available: https://ieeexplore.ieee.org/document/4099479/

[11] C. Wang, F. Grillot, and J. Even. *Impacts of Wetting Layer and Excited State on the Modulation Response of Quantum-Dot Lasers*. IEEE J. Quantum Electron. 48(9) (2012, Sep.) 1144–1150.
Available: http:// ieeexplore.ieee.org/document/6220843/

[12] P. Bhattacharya, J. Singh, H. Yoon, Xiangkun Zhang, A. Gutierrez-Aitken, and Yeeloy Lam. *Tunneling injection lasers: a new class of lasers with reduced hot carrier effects*. IEEE J. Quantum Electron. 32(9) (1996) 1620–1629.
Available: https://ieeexplore.ieee.org/document/535367/

[13] X. Zhang, A. Gutierrez-Aitken, D. Klotzkin, P. Bhattacharya, C. Caneau, and R. Bhat. *0.98-μm multiple-quantum-well tunneling injection laser with 98-GHz intrinsic modulation bandwidth*. IEEE J. Sel. Top. Quantum Electron. 3(2) (1997, Apr.) 309–314. Available: http://irepose.iitm.ac.in:8080/jspui/handle/11717/4416

[14] H. Yoon, A. L. Gutierrez-Aitken, R. Jambunathan, J. Singh, and P. K. Bhattacharya. *A 'cold' InP-based tunneling injection laser with greatly reduced Auger recombination and temperature dependence*. IEEE Photonics Technol. Lett. 7(9) (1995, Sep.) 974–976.
Available: https://ieeexplore.ieee.org/document/414673/

[15] P. Bhattacharya, S. Ghosh, S. Pradhan, J. Singh, Zong-Kwei Wu, J. Urayama, Kyoungsik Kim, , and T. B. Norris. *Carrier dynamics and high-speed modulation properties of tunnel injection InGaAs-GaAs quantum-dot lasers*. IEEE J. Quantum Electron. 39(8) (2003) 952–962.
Available: https://ieeexplore.ieee.org/document/1211140/

[16] G. Cerulo, L. Nevou, V. Liverini, F. Castellano, and J. Faist. *Tuning the dynamic properties of electrons between a quantum well and quantum dots*. J. Appl. Phys., 112(4) (2012) 43702.
Available: https://aip.scitation.org/doi/abs/10.1063/1.4746789

[17] S. Bhowmick, M. Z. Baten, T. Frost, B. S. Ooi, and P. Bhattacharya. *High Performance InAs/In$_{0.53}$Ga$_{0.23}$Al$_{0.24}$As/InP Quantum Dot 1.55 μm Tunnel Injection Laser*. IEEE Journal of Quantum Electronics. 50(1) (2014) 7-14.
Available: https://ieeexplore.ieee.org/document/6665003/

[18] H. Abbaspour, V. Ahmadi, and M. H. Yavari. *Analysis of QD VCSEL Dynamic Characteristics Considering Homogeneous and Inhomogeneous Broadening*. IEEE J. Sel. Top. Quantum Electron. 17(5) (2011, Sep.) 1327–1333.
Available: https://ieeexplore.ieee.org/document/5735154/

[19] F. Grillot, K. Veselinov, M. Gioannini, I. Montrosset, J. Even, R. Piron, E. Homeyer, and S. Loualiche. *Spectral analysis of 1.55 μmInAs-InP(113)B*

quantum-dot lasers based on a multipopulation rate equations model. IEEE J. Quantum Electron. 45(7) (2009, July) 872–878.
Available: https://hal.archives-ouvertes.fr/hal-00501878/document

[20] H. Jiang and J. Singh. *Strain distribution and electronic spectra of InAs/GaAs self-assembled dots: An eight-band study*. Phys. Rev. B. 56 (1997) 4696–4701.
Available: https://journals.aps.org/prb/abstract/10.1103/PhysRevB.56.4696

[21] C. Tong, D. Xu, and S. F. Yoon. *Carrier relaxation and modulation response of 1.3-µmInAs-GaAs quantum dot lasers*. J. Lightwave Technol. 27(23) (2009, Dec.) 5442–5450. Available: https://ieeexplore.ieee.org/document/5208395/

[22] T. W. Berg, J. Mork. *Quantum dot amplifiers with high output power and low noise*. Applied Physics Letters. 82(18) (2003, May) 3083-3085.
Available: https://aip.scitation.org/doi/10.1063/1.1571226.